The Effect of Forward Vehicle Velocity on Through-Body AUV Tunnel Thruster Performance

Aaron Saunders
Space and Subsea Robotics Laboratory
University of Victoria, Victoria, B.C.
Canada, V8W 3P6

Meyer Nahon
Department of Mechanical Engineering
McGill University, Montreal, Quebec
Canada, H3A 2K6

Abstract

New applications of streamlined Autonomous Underwater Vehicles require an AUV capable of completing missions with both high-speed straight-line runs and slow maneuvers or station keeping tasks. At low, or zero, forward speeds, the AUV's control surfaces become ineffective. To improve an AUV's low speed maneuverability, while maintaining a low drag profile, through-body tunnel thrusters have become a popular addition to modern AUV systems. The effect of forward vehicle motion and sideslip on these types of thrusters is not well understood. In order to characterize these effects and to adapt existing tunnel thruster models to include them, an experimental system was constructed. This system includes a transverse tunnel thruster mounted in a streamlined AUV. A 6-axis load cell mounted internally was used to measure the thrust directly. The AUV was mounted in Memorial University of Newfoundland's tow tank, and several tests were run to characterize the effect of vehicle motion on the transient and steady state thruster performance. Finally, a thruster model was modified to include these effects.

I. INTRODUCTION

Streamlined AUVs have traditionally been used in high-speed missions that require the vehicle to cover large distances or long missions that require high endurance. Tasks that involve precision positioning, have in most cases, been beyond the capabilities of streamlined AUVs. These missions generally make use of bluff bodied cage-style Remotely Operated Vehicles (ROV) which are much more maneuverable by virtue of their multiple thrusters mounted on the perimeter of the vehicle. Unfortunately this configuration dramatically increases the overall drag of the vehicle.

Streamlined AUVs generally use hydrodynamic control surfaces to steer the vehicle. These control surfaces lose their effectiveness at low speeds. In order to provide increased maneuverability at low speeds without changing the low drag profile of the AUV, through-body thrusters, also known as tunnel thrusters, can be added. Adding tunnel thrusters enables the vehicle to travel long distances at high speeds to a desired destination and then perform tasks that require station keeping such as environmental inspection. This effectively merges the maneuverability strengths of ROVs with the hydrodynamic efficiency of AUVs. Several AUVs such as the NPS ARIES [1], C-SCOUT [2], and REDERMOR [3] make use of tunnel thrusters for low speed maneuverability.

The C-SCOUT (Canadian Self-Contained Off-the-shelf Underwater Testbed) AUV [2] is part of a research project concerned with the development of AUVs for environmental missions in assessing the impact of discharges from offshore oil and gas operations. The project is based at the Memorial University of Newfoundland (MUN) and is being conducted jointly with the National Research Council's Institute for Marine Dynamics (IMD), McGill University, Petro-Canada, ISE Ltd., and Geo-Resources. The C-SCOUT was designed to be able to cruise ahead or astern with a high degree of maneuverability, and to hover, even in a cross-current. As shown in Figure 1, it is streamlined in shape, and has control planes for control while underway, and through-body tunnel thrusters for hover and low speed control.

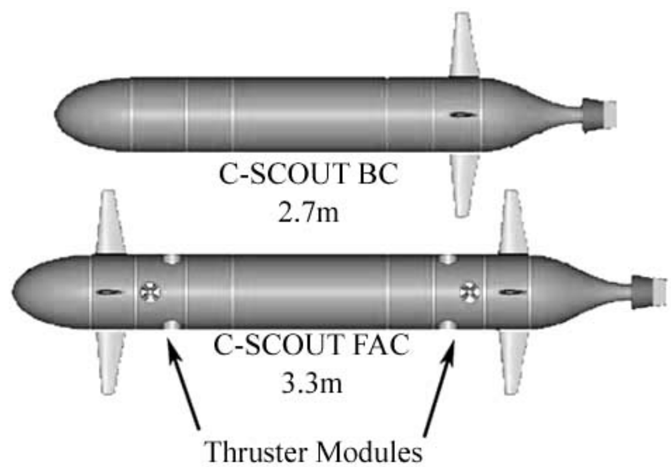

Figure 1. Top View of C-SCOUT Configurations; BC-Base Configuration, FAC- Fully Actuated Configuration

The design of the vehicle is to be accomplished in stages. The baseline configuration (BC) of the vehicle has four control surfaces aft, and a single thruster aft for propulsion. The fully-actuated configuration (FAC) has the four aft control surfaces, but also four control surfaces toward the front of the vehicle. In addition, the fully actuated version is equipped with six through-body thrusters: two thrusters are to be placed vertically; one forward and one aft, and the remaining four are to be placed horizontally two forward and two aft. The tunnel thruster placements give low-speed control in pitch, heave, yaw, roll, and sway, with surge control accomplished by the main propulsor. Presently the

0-7803-7535-1/$10.00©2002 IEEE

baseline configuration has been built and is undergoing tests at IMD.

The basic concept of through-body tunnel thrusters in AUVs is very similar to that of bow-thrusters used to maneuver large ships. It is therefore appropriate to mention the literature relating to bow thrusters, some of which dates back to the 1950's. These works deal primarily with steady-state bow thruster performance. For example, Beveridge [4] discusses the hydrodynamic forces and moments produced by bow thrusters, and reports that thruster effectiveness is reduced substantially during forward and astern travel relative to bollard pull conditions.

A good discussion of how thruster dynamics can affect URV (Underwater Robotic Vehicle) control is presented by Yoerger, Cooke and Slotine [5]. They concluded that the dynamics of underwater vehicles can be dominated by the thruster dynamics, especially during low speed or hover operation. They also suggest that if compensation for these dynamics are not included in the control system, the closed-loop system will be bandwidth limited and may lead to limit cycling behavior, which reduces the ability of the vehicle to perform precise station keeping tasks. It therefore becomes important to assemble an accurate dynamic thruster model in order to design the system controller.

Most naval architecture and marine engineering texts (e.g. [6]), apply momentum theory to derive a model for a thruster's steady state axial thrust. They show that this thrust varies with the square of the flow velocity through the propeller. This theory does not include the details necessary to capture the effects of blade shape. To capture this detail, blade element theory uses lift and drag forces generated from each element of the blade cross section, summed over the total length of the blade. To use this method, a representation of the lift and drag curves as a function of the incident flow angle is required. This information is readily available from aerodynamic design texts for a large variety of airfoil cross-sections for small angles of attack [7]. During thrust reversal, the local angle of attack spans a full 360 deg. Rickards [8] discusses how these nominal lift and drag curves can be created by ignoring the discontinuities that arise during blade stall. This then allows full flow reversal to be modeled using simplified single term sinusoidal functions [9] [10].

An alternative approach is to use propeller specific dimensionless thrust and torque coefficients. The coefficients are related to the advance velocity and rotational speed of the propeller, and are often referred to as 'open water propeller data'. This data can be presented for four-quadrants of propeller operation, based on the relative directions of advance velocity and propeller rotation. First quadrant data for most types of modern day propellers is readily available, but full four-quadrant data is hard to find. Fossen [11] describes a method using a linear approximation of thrust and torque coefficients to represent four-quadrant thrust. Fossen also reports that under heavy transients this method can be up to 40% erroneous. To use these types of non-dimensional coefficients accurately, extensive experimental data would be required. One of the first attempts to look at this data in depth was by Lammeren, Manen and Oosterveld [12]. Data for the Wageningen B-Series propellers was fitted by a 20 term Fourier series to enable numerical representation of the full four-quadrant thrust and torque coefficients. While this is valuable for B-Series open propellers, it is not directly transferable to other propellers such as the shrouded Kaplan typically found on URVs.

Several dynamic models have been developed to represent the transient performance of tunnel thrusters using momentum theory with a blade element model for the propeller. A historical summary of recent work in lumped-parameter thruster dynamics modeling is given by Whitcomb and Yoerger [13]. The first work directly related to small AUV tunnel thrusters was done by McLean [14] at the Naval Postgraduate School on the AUV II tunnel thruster. Brown [10] [15] adapted McLean's momentum based model to use the blade element, lift/drag, theory to model the propeller in a tunnel thruster model. Models presented by Bachmayer, et al. [9] [16] later expanded the basic four-quadrant models to include additional fluid effects such as rotations and presented a method for experimentally determining nonsinusoidal lift/drag curves.

An important step in modeling the performance of any physical system is validating the numerical model. The experiments completed in [9] [14] [15] and [17] made use of small tanks or water channels to measure the performance of a stationary thruster. In Brown's model [15], four parameters tied to the specific design of the tunnel and propeller were determined empirically by matching the computer simulation with the experimental axial force data. The experimental setup in [9] and [17] used a more sophisticated 6-axis load balance setup for measuring axial thrust and hydrodynamic torque. Those works also used a 3-D Doppler flow meter to measure flow velocities at the thruster intake and outlet, which allowed the estimation of empirically derived lift/drag coefficient curves.

Presently, the models mentioned above do not include the effects of forward vehicle motion or vehicle orientation on through-body thruster performance. In order to adapt existing tunnel thruster models to include these effects, an experimental system was built to characterize the effects of forward vehicle speed and yaw angle on tunnel thruster performance. This system includes a transverse tunnel thruster mounted in a model of the C-SCOUT AUV and a 6-axis load cell mounted internally to measure thrust. The model was mounted in Memorial University of Newfoundland's tow tank. This paper discusses the experimental setup, the results obtained from tow tank testing, and the incorporation of these results into a computer simulation.

II. EXPERIMENTAL SYSTEM

A. Thruster and Controller

Figure 2 shows the layout of the thruster system. The major components include:

- Personal Computer (PC) running LabVIEW software for the control and data acquisition user interface.

- Keithley PCI Data Acquisition Card (DAC), interface to the Maxon controller
- Maxon servo amplifier/controller
- Thruster Unit: Maxon servomotor, gearbox, propeller
- ATI Force/Torque load cell and ISA controller card to power the load cell and convert the raw sensor data into 6-axis force information.

The Maxon motor and controller contain an internal speed sensing and control loop allowing the motor to be driven by commands in rotational speed, rather than by current commands as in [10] and [15].

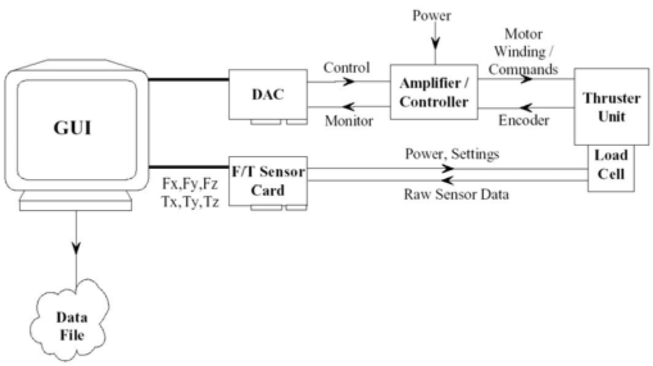

Figure 2. Thruster System Schematic

Figure 3 shows the general layout of the thruster components. The tunnel thruster unit consists of the following major components: Maxon Servomotor, Reduction Gearbox (5:1), Thruster Leg, Propeller, and a 4 in ID PVC Tunnel.

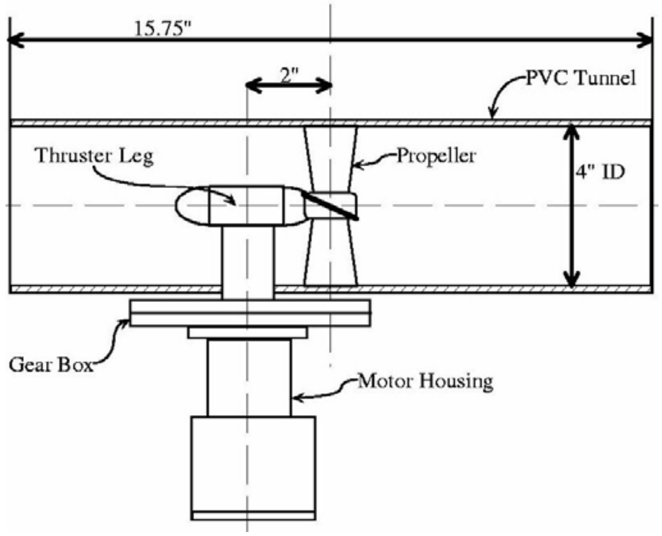

Figure 3. Tunnel Thruster Layout

A custom propeller was fabricated at IMD due to the difficulties in locating an off-the-shelf propeller for the 4 in tunnel diameter. The propeller is a four blade Kaplan style propeller with unity pitch to diameter ratio; blade area ratio of 0.55; 100.3 mm (3.95 in) OD; and 23.8 mm (0.9375 in) hub diameter.

In order to test the tunnel thruster in the full scale C-SCOUT, all the thruster components including the load cell needed to be mounted inside a 0.305 m (12 in) long tunnel thruster module. The resulting module is shown in Figure 4.

An ATI Gamma multi-axis force/torque (F/T) sensor was used to measure the required thruster loads. This transducer had ranges of ±133.4N (±30 lb) in F_x and F_y; ±445N (±100 lb) in F_z; and ±11.3Nm (±100 in-lb) in all three torque axes.

In the experimental system, a crucial issue in mounting the thruster unit into the module is ensuring the mechanical isolation of the thruster unit from the module (or hull). Because the load cell is measuring the forces generated by the entire thruster unit, any contact between the hull and tunnel entrances would result in incorrect load information. The tunnel entrances were designed to match the hull shape and be offset by 1/16 in. The design of the intakes was not optimized---they simply match the hull curvature and have 7/8 in. rounded edges.

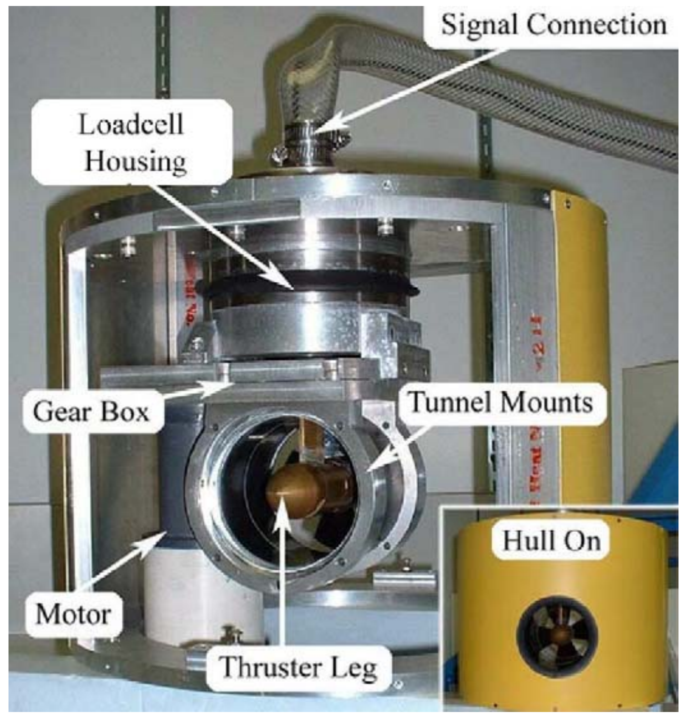

Figure 4. Thruster Module

The module was bolted directly into a model of the C-SCOUT AUV, and the entire model was mounted to a yaw assembly and mounted on the tow tank carriage. The AUV model used for these experiments was a full scale replica of the C-SCOUT vehicle. This model was built at IMD to enable research on the hydrodynamic properties of the C-SCOUT and various types of propulsion systems currently being developed.

B. Tow Tank

Figure 5 shows the configuration of the C-SCOUT model as mounted on the tow carriage. The model was moved through the water at various constant yaw angles and speeds in the MUN tow tank in order to quantify the effects of vehicle speed and orientation on thruster performance. The tow tank is 54.7 m long (~32.2 m usable), 4.57 m wide with an adjustable water depth up to 2.5 m and a top carriage speed of 5.0 m/s. The C-SCOUT model had to be held below the water and set at various yaw angles. To do this, a Yaw

Frame was designed to mount to the tow carriage load points and hold the two struts on the C-SCOUT model, as shown in Figure 5. The lower half of the yaw frame could be rotated and fixed through ±90° of rotation in 5° increments.

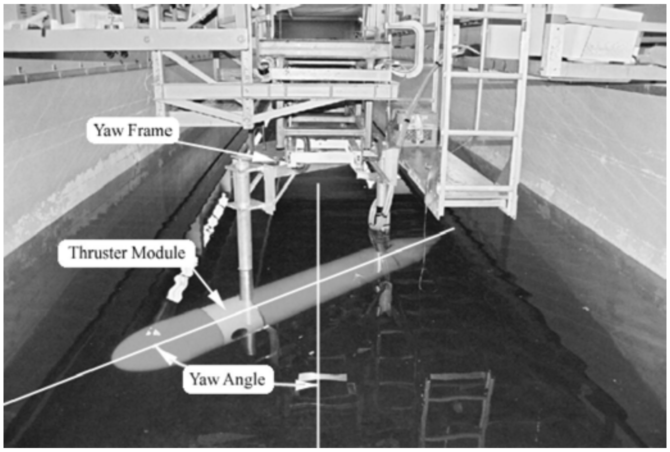

Figure 5. TowTank

III. EXPERIMENTAL RESULTS

A. Test Procedure

The testing in this work focussed on a single tunnel thruster module mounted in one location on the vehicle. It is expected that hull interaction will play a large role in the experimental results. Testing one location on the vehicle will only provide information for that location and the data obtained may not be applicable to other thruster locations. In addition, the results may be vehicle dependent and therefore may not be directly applicable to other vehicles. A test procedure was developed to ensure that the desired information would be captured in the test results. The C-SCOUT vehicle was designed to have a top forward speed of 4 m/s. The operational range of the vehicle investigated in this work can be split into three regimes:

- Maneuvering/hovering, in cross currents up to 0.5 m/s
- Forward Travel - zero yaw angle forward travel
- High Speed Turning with side-slip

It was important to create a test matrix to cover all three regimes of operation. It was also important to obtain both steady state and transient test data for each regime. By testing yaw angles between ±90° at speeds up to 0.5 m/s the entire Maneuvering range is satisfied. Testing up to 4 m/s at zero yaw angles covers the Forward Travel condition. The last regime is the high speed turns with side-slip. The yaw frame was not designed to hold the vehicle against large hydrodynamic loads experienced during large yaw angles and high forward speeds. It was therefore necessary to minimize the range of angles tested at higher speeds. It was estimated that, during C-SCOUT operation, a maximum-rudder turn at a forward speed of 1.5 m/s would result in a side-slip angle of 20°. The High Speed Turning range was therefore selected to include this point. A pictorial representation of the resulting test matrix can be seen in Figure 6. In total, there are 86 test cases for each the steady state and transient tests.

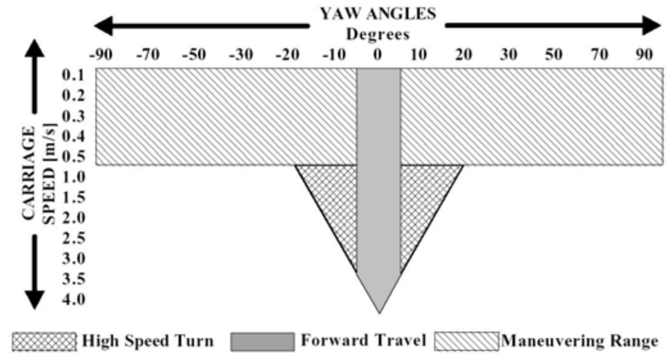

Figure 6. Test Matrix

B. Steady-State Results

Prior works have shown that a thruster's steady state thrust is proportional to the square of the propeller RPM [5] [9] [10] [13] [17]. This was verified in the present work, as shown in Figure 7. However, it was noted that the constant of proportionality (slope of Fig. 7) is 26.7% higher for reverse RPM than for forward RPM. This is no doubt due to the asymmetric geometry of the thruster leg arrangement, shown in Figure 3, and of the propeller section.

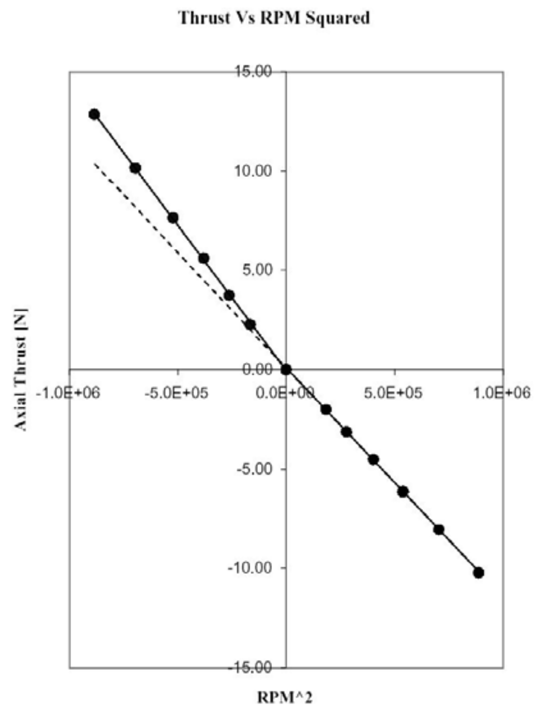

Figure 7. Steady-State Static Thrust Results

For the steady state tests in the tow tank, the thruster unit was always operated in a positive rotational direction, which results in water flow from left to right in Figures 3 and 8(a). When oriented at +90° yaw angle, Figure 8(c), the oncoming water is coming in the same direction as the thruster tries to drive it. As will be seen, this causes a decrease in thrust because the propeller RPM is much higher before its advance velocity matches the speed of the oncoming water. In Figure 8(b), at -90°, the opposite occurs: the water exiting the thruster is being pushed into the oncoming water. It is expected that these complicated flow conditions will have a large effect on the thruster performance. The only important assumption made before starting the tests is that the asymmetry in the thrust will remain the same as in the static tests. This allows us to use the slope difference for the stationary tests (Figure 7) to convert the positive rotation propeller data into negative rotation.

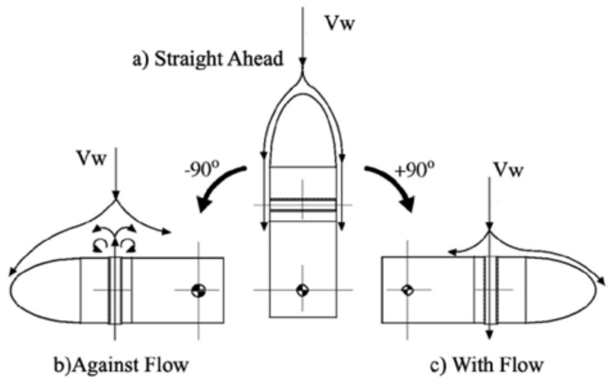

Figure 8. Flow Cases

It would take a very long time to complete an individual test matrix for several steady-state propeller speeds. In order to reduce test time, the motor speed was slowly ramped from zero to full speed for each constant forward speed and yaw angle from the test matrix. Several values on the ramp were compared to true steady state thrust and the values matched closely. It was therefore assumed that the data from the slow ramp, was an accurate representation of the steady state performance.

Axial thrust is again plotted against propeller RPM squared. Figure 9 shows two sample plots (for V = 0.4 m/s, Yaw = ±50˚) from the test matrix. The linear relationship between axial thrust and RPM squared still appears to hold when the vehicle is yawed and moving forward. However, it is apparent from Figure 9 that the y-intercept is no longer zero but varies with orientation and carriage speed. The relationship between steady state thrust and RPM squared therefore becomes

$$F_a = a + b\omega_p \left|\omega_p\right| \quad (1)$$

where F_a is the axial thrust, a is the y-intercept in [N], b is the slope in [N/RPM^2], and ω_p is propeller speed in [RPM].

The fact that all the steady state experimental data follows the relationship given by eq. (1) indicates that we can study these results simply by looking at how a and b vary with forward speed and yaw angle. For each test case, the slope and y-intercept were extracted, and the results are plotted in Figures 10 and 11 for test cases in the Maneuvering range.

Maneuvering: The Maneuvering range contains the bulk of the experimental tests. In general, axial thrust performance is reduced slightly as carriage speed is increased, as shown in Figure 11. At low speeds, the slope values do not change much as a function of yaw angle. As carriage speed is increased, the magnitude of the slope falls more quickly with speed. For yaw angles between -50˚ and -70˚ there is a dramatic drop in axial thrust performance, to about half the low speed value. This is thought to be caused by the fluid interaction at the thruster outlet and the disturbance to the inlet caused by the body of the vehicle. This is not of great concern, considering that a negative yaw angle and a positive propeller speed correspond to the thruster trying to move the vehicle in the same general direction as the oncoming flow---not a likely occurrence in a station-keeping or hovering operation.

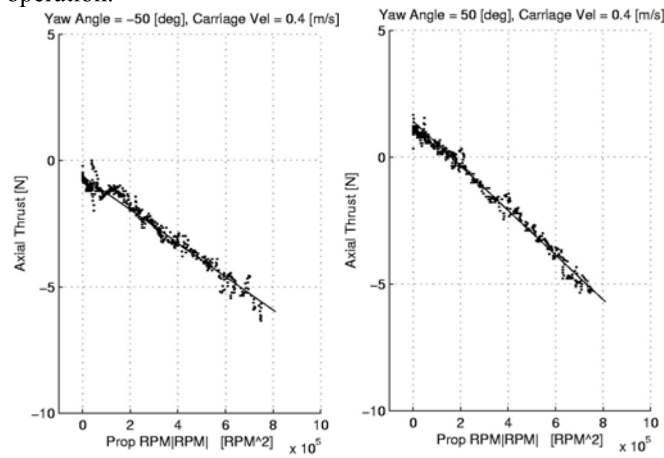

Figure 9. Steady-State Static Thrust Results

The behavior of the y-intercept is relatively intuitive: as the component of the oncoming speed along the thruster's longitudinal axis increases (increasing speed, increasing yaw angle), the load cell senses a force in that same direction. When the yaw angle is negative, the y-intercept is also negative and increases in magnitude with increasing speed. Between ±30˚, the intercept curves do not appear to be affected much by forward velocity. At larger yaw angles and higher speeds, the intercept becomes more significant.

The complexity of the curves in Figures 10 and 11 suggest that there is no simple relationship between forward speed, yaw angle and axial thrust. It is likely that the complex fluid dynamical effects of hull interaction have a large effect on thruster performance. As a result, the performance characteristics of the tunnel thruster cannot be de-coupled from the C-SCOUT model, making the data vehicle dependent.

Forward Travel: The intercept and slope data for the high speed tests at zero yaw angle are not shown here, due to space constraints. Because the vehicle is completely symmetrical about its longitudinal plane, the pressure at the tunnel intake and exit should be the same, resulting in zero net flow though the tunnel at zero RPM. Therefore, the y-intercept a should remain zero for the full range of speeds. The intercept values are very close to zero at low speeds but then become significant beyond 1.0 m/s, and appear to increase quadratically with forward speed (reaching 3.5 N at 4 m/s). It is suspected that a misalignment of the vehicle model with respect to the direction of travel of the tow carriage caused this to occur. Based on the fact that the plots of a versus yaw angle crossed zero at the same location (-7˚) for all values of forward speed, it would appear that the model was misaligned by that angle. At the time of the tests, a series of indirect measurements was relied upon to align the vehicle, but a misalignment of 7˚ between the vehicle (1.75 m below the carriage) and the carriage is plausible. We therefore expect that the values of intercept should, in reality, be close to zero for all vehicle speed at zero yaw angle. There was no clear pattern in the slope data for the high speed tests at zero yaw angle. The raw data for these tests was relatively noisy, and we attribute this to the structural flexibility of the yaw frame. From the data, it seems reasonable to assume that the slope *b* remains constant (at about -1.1×10^{-5} N/RPM^2) in this range.

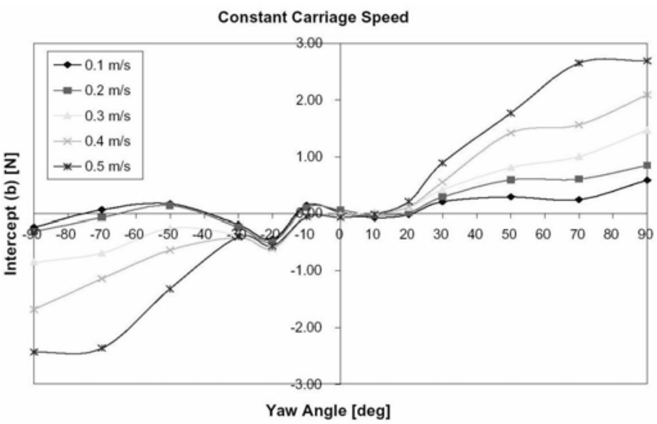

Figure 10. Maneuvering Range Axial Thrust Intercept Values

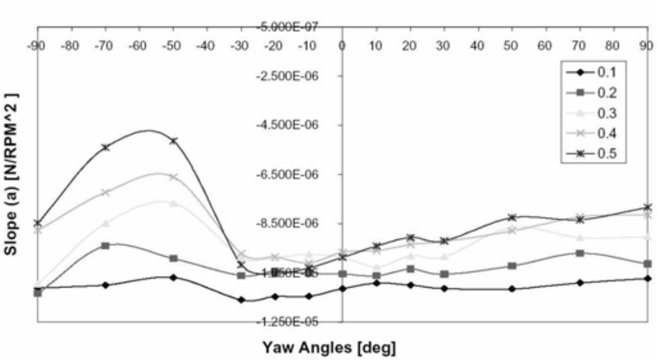

Figure 11. Maneuvering Range Axial Thrust Slope Values

High Speed Turns: Although the tunnel thrusters were not intended to be used at higher speeds they may be a useful means of control augmentation. It has been shown by Ridley [18] that bow thrusters are an effective steering aid in surface ships with headway. It is assumed that a similar effect would apply to underwater vehicles using tunnel thrusters. For positive yaw angles there appears to be a slight increase in the axial thrust produced for a given RPM when compared to the straight ahead case. This is actually the opposite of the effect observed at lower speeds in Figure 11. For negative yaw angles, the opposite is true: increasing forward speed leads to a reduction in thrust. Additionally, the magnitude of this reduction does not seem to be constant with increasing yaw angles. One interesting feature in the intercept data is the lack of symmetry about the zero-yaw case (even if shifted by -7˚). This is attributed to the asymmetrical configuration of the internal thruster components (e.g. thruster leg). Because this imbalance is significant, it would suggest that having a fully symmetrical tunnel configuration would be beneficial.

C. Transient Test Results

In order to capture the thruster's transient behavior, square wave commands in RPM were used. The same test matrix was used for the transient tests as in the steady state tests (Figure 6). At each of these conditions the thruster was cycled through a series of alternating step inputs from forward speed to reverse speed. In general, the transient behavior did not change significantly with yaw or forward speed. For example, Figure 12 shows the response of the thruster for several values of forward speed (0.1 to 0.5 m/s) at 30˚ yaw. The overall shape and magnitude of the different curves match closely. The only significant difference between the curves is the reduction in steady state thrust as carriage speed is increased. This issue was addressed in some detail in the previous section. The close match between transients was also observed at higher carriage speeds, and over the full range of yaw angles. From this, we can conclude that forward speed and orientation do not have a significant effect on transient thruster performance, and that static transient thruster tests can be used to define the transient performance of the tunnel thruster unit.

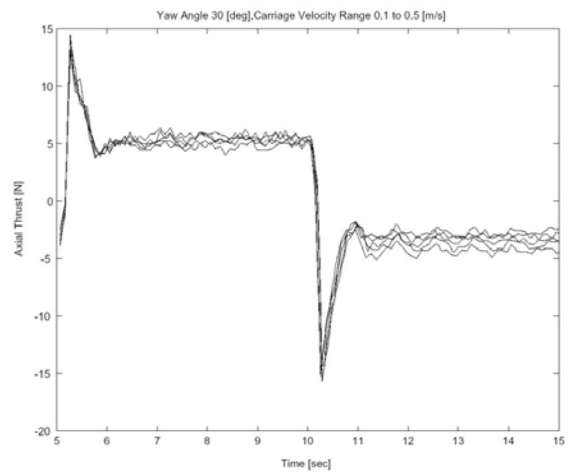

Figure 12. Square Wave Response

IV. MODELING

This section reviews an existing tunnel thruster model which is then adapted to include the effects of vehicle speed and orientation, based on the experimental results from Section III.

A. Basic Model

Our 'basic' model is loosely based on the work by Brown [15] and Healy et al. [10]. A block diagram of their model is shown in Figure 13. The original model included two coupled nonlinear first order differential equations, and thus two state variables. Whitcomb and Yoerger [13] showed that when the motor is equipped with an internal speed sensing loop, the model is reduced to only a single first order differential equation with a single state variable: the fluid velocity at the propeller U_a. Accordingly, since our setup uses propeller speed as the control input, the upper part of the block diagram shown in Figure 13 was no longer needed.

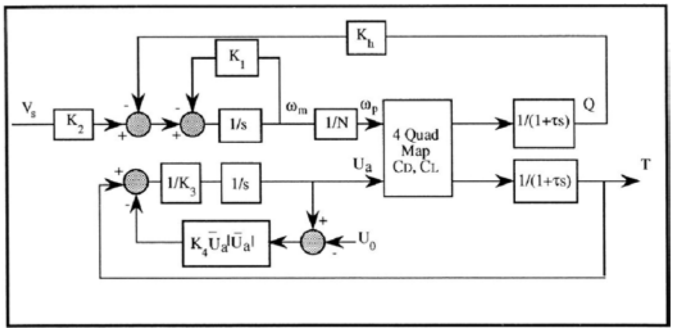

Figure 13. Brown's System Model [15]. Note that some symbols in this diagram do not correspond to those used in this paper.

The reduction in model order from two to one state variables removes the uncertainties involved in modeling the electro-mechanical system by using the speed sensor feedback from the motor. However, it relies on having a robust inner motor speed loop which can be relied on to provide the commanded propeller speed accurately and with no lag. This corresponds to our experimental setup, and leads to our 'basic' model governed by a single differential equation:

$$F_a = K_1\dot{U}_a + K_2 U_a \left|U_a\right| \tag{2}$$

where $K_1 = \rho A l \gamma$ and $K_2 = \Delta\beta\rho A$. U_a is the fluid velocity at the propeller, F_a is output thrust, ρ is the water density, A and l are the duct area and length, γ is an empirically determined added mass coefficient, and Δβ is a momentum flux coefficient [15]. The resulting model block diagram is shown in Figure 14. In eq. (2), the output thrust is seen to consist of two components. The first term on the right-hand-side corresponds to the transient effects, while the second term corresponds to the steady-state thrust. It can also be shown that the second component can also be written in the form given by eq. (1), with $a = 0$, for the case of a static thruster.

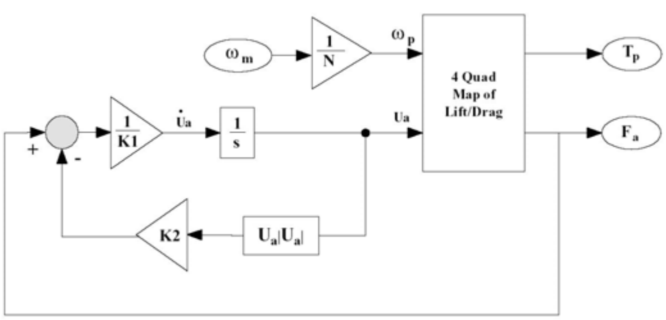

Figure 14. The Basic Model

It is important to note the limitations of the models discussed above. The basic model is unable to model a thruster moving with forward speed in a yawed orientation. This can be traced to the fact that (a) the governing equations were developed with the assumption that the ambient water velocity is zero, and (b) the model presumes symmetry in the thruster's performance with respect to positive/negative RPM. This latter assumption is clearly flawed, as seen in the experimental data shown in [10] and [15], and as was evident in the data shown here earlier.

B. Modeling the Effects of Forward Speed and Yaw

The most significant limitation of the model presented in the previous section is its assumption of zero ambient axial water velocity. This section discusses a means for including the effects of forward speed and orientation into the tunnel thruster model. In order to model a thruster that is moving through the water with a vehicle, the effect of the inlet water velocity must be taken into consideration. The model presented by Blanke et al. [19] included the effects of nonzero vessel speed relative to the water. That model is developed in much the same way as Brown's model [15], with the exception that it does not assume a zero ambient water velocity. In this case, we find that the development leads to

$$F_a = K_1\dot{U}_a + K_2(U_a - U_\infty)\left|U_a\right| \tag{3}$$

where U_∞ is the ambient axial water velocity. In ship modeling. U_∞ is usually equivalent to the forward vessel speed. The addition of vessel speed will improve the accuracy of the model for a thruster whose axis is parallel to the direction of travel. However, with a through-body thruster, the thrust axis is seldom parallel to the direction of travel, and so the effect of vehicle orientation must also be taken into account.

In order to capture effects of forward speed and orientation, we return to the experimental results presented in Section III. It was observed there that forward speed and orientation had little effect on the transient behavior of the thruster. This allows us to keep the transient portion of eq. (2) intact and concentrate on modifying the steady state portion. It was shown that the experimental steady state results could be condensed into the relationship given by eq. (1). By replacing the steady state portion of eq. (2) by eq. (1), we obtain the following first order differential equation

$$F_a = K_1\dot{U}_a + a + b\omega_p\left|\omega_p\right| \tag{4}$$

C. Augmented Model

The approach discussed in the preceding section allows us to capture the effects of forward speed and yaw angle in an 'Augmented Model'. The key differences between the basic and augmented models are as follows:

- The effects of forward vehicle speed and orientation are included by using the experimental results from tow tank testing. This is achieved through the use of lookup tables for a and b over the entire range of forward speeds and yaw angles tested in this work.
- The effects of asymmetry in transient thruster performance are captured by tuning γ separately for the forward and reverse axial flow case. In the simulation, the direction of axial water flow, U_a, is evaluated at each pass through and the appropriate forward or reverse γ is used.

Non zero values of a are due to the forces in the thruster unit for $\omega_p = 0$. As shown in Figure 10, a is a function of yaw angle and forward speed. The value of b is a function of yaw angle, forward speed, and the direction of U_a. In particular, we must account for the direction of U_a relative to a particular forward speed and yaw angle, as shown in Figure 8. The tow tank tests were run for yaw angles in the range of ±90º, but always for positive ω_p ramps. Therefore, the values of b available are for one direction of U_a corresponding to a particular yaw angle and forward speed. We presume that the value of the slope b for negative ω_p at a particular speed and yaw angle is the same as for positive ω_p at the same speed but the negative yaw angle. In addition to this, the value of b must be modified if ω_p is in the negative direction to account for the asymmetry in steady state thrust, shown in Figure 7. This is done by multiplying b by a modifier, b_{Mod}, which corresponds to the increase in the slope of b observed in the steady state tests for negative ω_p. The resulting model is shown in Figure 15.

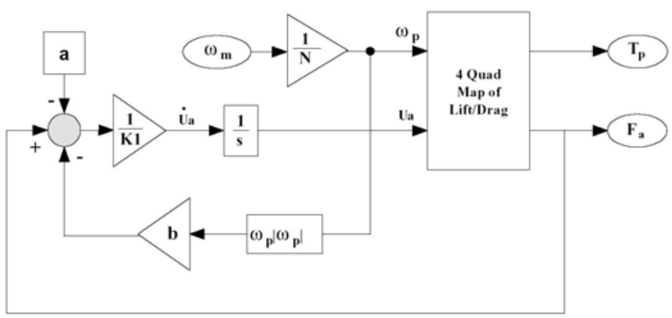

Figure 15. The Augmented Model

D. Simulation Results

We are now in a position to compare the capabilities of the basic and augmented models. It is important to note the method of identification for different model parameters. In the basic simulation, there are four parameters that must be manually selected: γ, the added mass coefficient; Δβ, the momentum flux coefficient; C_{Lmax}, the maximum lift coefficient; and C_{Dmax}, the maximum drag coefficient. This is referred to as 'tuning the model'---a process by which the model parameters are varied until the simulation output matches an experimental data set. In general, the axial force transient peak was matched by adjusting γ and C_{Lmax}, the steady state thrust by adjusting Δβ and C_{Lmax}, and finally the propeller hydrodynamic torque load by adjusting C_{Dmax}. Because the parameters cannot be tuned independently, their final values are somewhat arbitrary. However, it is important to ensure that the values stay within their physically meaningful range. For example, Δβ cannot exceed 2 (its ideal value, predicted by momentum theory); for low aspect ratio wing section, C_{Lmax} rarely exceeds 1.0; and the flat plate drag C_{Dmax} will generally not exceed 2. With these ranges defined, the basic model was manually tuned and the resulting parameter values are presented in Table 1. For the present purpose, the model was tuned to match the forward steady state thrust as closely as possible.

Figures 16(a) and 17(a) show the response to a slow positive ramp input and to a square wave input in ω_p, respectively, for V = 0.1 m/s and Yaw = 0. Under these conditions, the basic model does a reasonable job of matching the experimental data, though it does miss the asymmetry in steady-state performance (positive plateaus in Figure 17(a). This observation, in addition to the transient tow tank results, supports the idea that only the steady state portion of the model needs to be replaced. Under more extreme conditions of V = 0.5 m/s and Yaw = 90°, shown in Figures 18(a) and 19(a), the basic model's performance is much less satisfactory. Both Figures 18(a) and 19(a) show a significant mismatch in steady state and transient thrust between the basic model and experimental data.

Parameter	Value	Units	ID Method
D	0.1016	m	measured
l	0.410	m	measured
A	0.00811	m^2	measured
γ	1.2	--	Tuned
Δβ	1.7	--	Tuned
ρ	998	kg/m^3	handbook
C_{Lmax}	0.6	--	Tuned
C_{Dmax}	1.125	--	Tuned
ϕ	0.4268	rad	measured

Table 1. Basic Model Parameters

We now turn our attention to the augmented model. For this simulation there are only three tuned parameters: γ, C_{Lmax} and C_{Dmax}. Because the propeller geometry has not changed, there is no justification for changing the value of C_{Lmax} or C_{Dmax} from the basic model. This leaves only one variable to tune: γ, which will have a different value for forward and reverse axial flow directions.

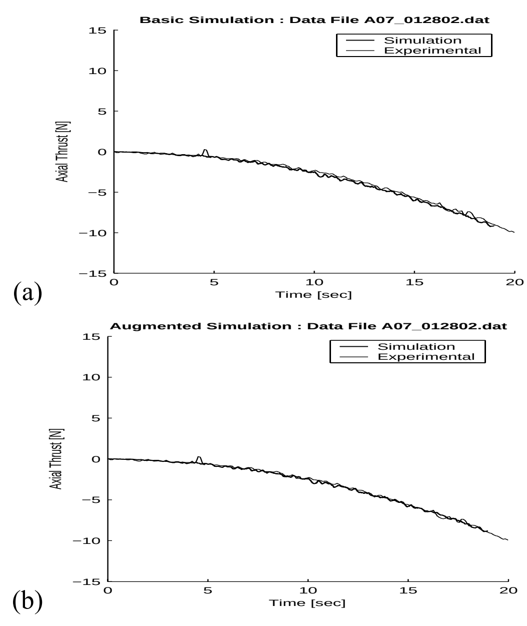

Figure 16. Slow Ramp Response, V = 0.1 m/s, Yaw = 0

In general, an increase in γ results in an increase in thrust overshoot and settling time. Values for forward and reverse γ were obtained by tuning the model for the stationary thruster case. The new additions to the model are the experimentally fitted values of intercept and slope, a and b, from Figures 10 and 11. These values were integrated into the simulation using lookup tables. Overall, the augmented model requires less tuning due to the addition of the lookup tables. The resulting parameter values for the augmented simulation are presented in Table 2.

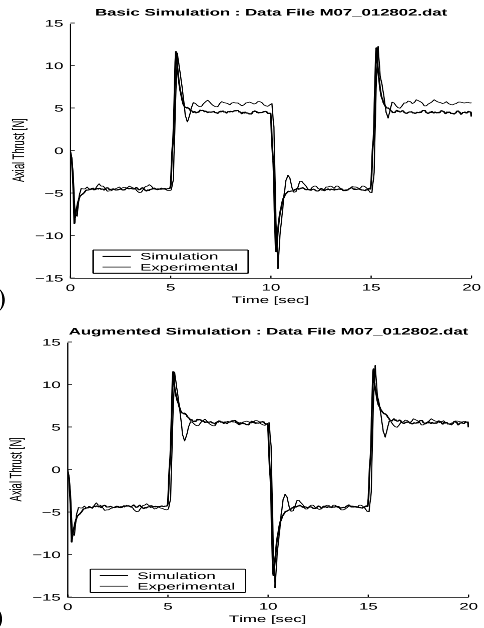

Figure 17. Square Wave Response, V = 0.1 m/s, Yaw = 0

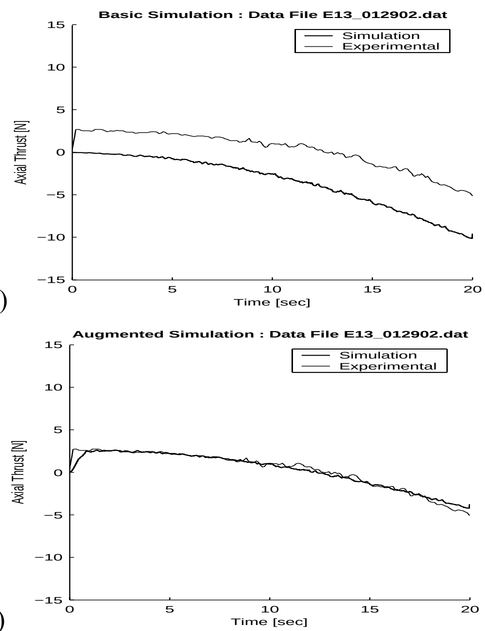

Figure 18. Slow Ramp Response, V = 0.5 m/s, Yaw = 90°

In order to demonstrate the capabilities of the augmented model, the same test cases are considered as for the basic model. Figures 16(b) and 17(b) show the response to a slow positive ramp input and to a square wave input in ω_p, respectively, for V = 0.1 m/s and Yaw = 0. Here, the results from the augmented model match the experimental data quite well, including the asymmetry in steady-state performance (positive plateaus in Figure 17(b)). For the more extreme conditions of V = 0.5 m/s and Yaw = 90°, shown in Figures 18(b) and 19(b), the augmented model's performance is again very good. This was true, in general, for all conditions, the exceptions being at large yaw angles and speeds above 0.4 m/s. Figure 19(b) shows that the settling time of the predicted thrust overshoot does not match the experimental data at these conditions. This mismatch at large yaw angles is most likely due to the error in fitting the *a*'s and *b*'s to the experimental thruster data by the large amount of scatter for these more extreme test cases. The model was, however, able to capture the asymmetry in transient behavior very well.

In summary, the results from the augmented simulation are well within acceptable limits for representing the performance of the tunnel thruster during forward speed and yawed orientation. The small mismatches in modeled performance would most likely have little or no effect on the vehicle's overall operation.

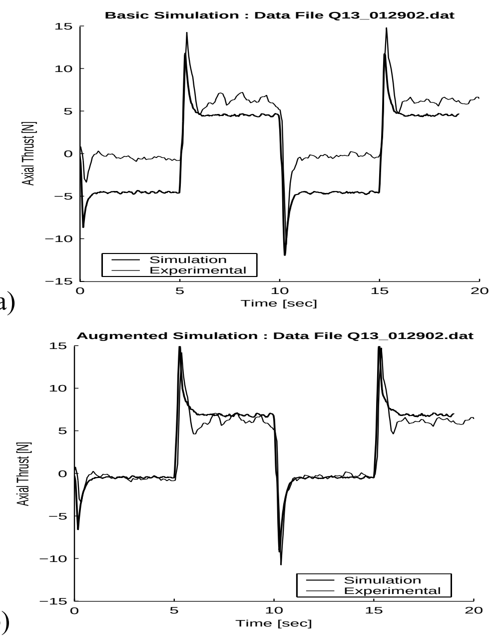

Figure 19. Square Wave Response, V = 0.5 m/s, Yaw = 90°

Parameter	Value	Units	ID Method
D	0.1016	m	measured
L	0.410	m	measured
A	0.00811	m^2	measured
γ_F	0.6	--	tuned
γ_R	0.9	--	tuned
ρ	998	kg/m^3	handbook
C_{Lmax}	0.6	--	tuned
C_{Dmax}	1.125	--	tuned
ϕ	0.4268	rad	measured
A	lookup	N	measured
B	lookup	$N/(rad/s)^2$	measured
b_{Mod}	1.267	--	measured

Table 2. Augmented Model Parameters

V. Conclusions

A small tunnel thruster was constructed, mounted in an AUV and tested in a tow tank at various forward speeds and yaw angles. Overall, the tow tank testing revealed that the effects of yaw and forward speed are fairly complex, suggesting that complicated fluid dynamics effects dominate steady state thruster performance. The linear relationship between axial thrust and propeller rotational speed squared was found to hold for the full range of conditions. The steady state tests revealed that (a) thruster performance during low speed maneuvering is only slightly reduced by forward speed, and that this decrease in steady state thrust becomes more pronounced as the yaw angle is increased; (b) there exists a definite asymmetry in thruster performance with respect to positive/negative yaw angles; and (c) there exists a distinct asymmetry in thruster performance with respect to positive/negative RPM. The transient test results were relatively unaffected by forward speed and yaw angles, but there existed a distinct asymmetry in response with respect to positive/negative RPM.

It was shown that existing tunnel thruster models do not capture asymmetry in axial thrust performance, and definitely cannot model the effects of forward speed and yaw angle. A new tunnel thruster model was assembled, loosely based on existing thruster models. Because the transient behavior did not change significantly with yaw angle and forward speed, only the steady state portion of the thruster model needed to be modified. The coefficients *a* and *b*, extracted from the experimental data were used directly to replace the steady state part of the tunnel thruster model. Asymmetry in transient behavior was handled by separately tuning the added mass coefficient for the forward and reverse axial flow conditions. The new model was successful in capturing the effects of forward speed and yawed orientation as well as asymmetry in thruster performance.

Acknowledgements

The authors gratefully acknowledge the financial support of the Natural Sciences and Engineering Research Council for this work. As well, we wish to thank Chris Williams and Tony Randell at the NRC Institute for Marine Dynamics and Neil Bose and Jim Gauss of MUN for their help in the use of IMD and MUN facilities.

References

[1] Marco, D. and A. Healey, 2000, 'Current Developments in Underwater Vehicle Control and Navigation: The NPS ARIES AUV', In: *OCEAN 2000 MTS/IEEE Conference Proceedings*, Providence, RI.

[2] Curtis, T., D. Perrault, C. Williams, and N. Bose, 2000, 'C-SCOUT: A General-Purpose AUV for Systems Research', Presented at *Underwater Technology 2000*.

[3] Mailfert, G. and J. LeMaire, 1998, 'REDERMOR: an Experimental platform for ROV/AUV field sea trial', In: *OCEANS'98 IEEE Conference Proceedings*, Nice, France.

[4] Beveridge, J., 1972, 'Design and Performance of Bow Thrusters', *Marine Technology,* 9 (4), 439–453.

[5] Yoerger, D., J. Cooke, and J. Slotine, 1990, 'The Influence of Thruster Dynamics on Underwater Vehicle Behavior and their Incorporation Into Control System Design', *IEEE Journal of Oceanic Engineering,* 15 (3), 167–178.

[6] Clayton, B. and R. Bishop, 1982, *Mechanics of Marine Vehicles*, Gulf Publishing Company.

[7] Abbott, I. and A. von Doenhoff, 1949, *Theory of Wing Sections*, McGraw-Hill.

[8] Rickards, M., 1970, 'Cycloidal Propulsion of Submersibles', *Journal of Hydronautics* 4 (2), 66–72.

[9] Bachmayer, R., D. Yoerger, and M. Grosenbaugh, 2000, 'An Accurate Four-Quadrant Nonlinear Dynamical Model for Marine Thrusters: Theory and Experimental Validation', *IEEE Journal of Oceanic Engineering,* 25 (1), 146–159.

[10] Healey, A., S. Rock, S. Cody, and J. Brown, 1995, 'Toward an Improved Understanding of Thruster Dynamics for Underwater Vehicles', *IEEE Journal of Oceanic Engineering,* 20 (4), 354–361.

[11] Fossen, T., 1994, *Guidance and Control of Ocean Vehicles*, John Wiley and Sons Ltd.

[12] van Lammeren, W., J. van Manen, and M. Ooseterveld, 1969, 'The Wageningen B-Screw Series', *SNAME Transactions,* 77, 269–317.

[13] Whitcomb, L. and D. Yoerger, 1999, 'Development, Comparison, and Preliminary Experimental Validation of Non-Linear Dynamic thruster Models', *IEEE Journal of Oceanic Engineering*, 24 (4), 495–506.

[14] McLean, M., 1991, 'Dynamical Performance of Small Diameter Tunnel Thrusters', Master's Thesis, Naval Postgraduate School, Monterey, California.

[15] Brown, J., 1993, 'Four Quadrant Dynamical Model of the AUV II Thruster', Master's thesis, Naval Postgraduate School, Monterey, California.

[16] Bachmayer, R., M. Whitcomb, and M. Grosenbaugh, 1998, 'A Four Quadrant Finite Dimensional Thruster Model', In: *OCEANS'98 IEEE Conference Proceedings*, Nice, France.

[17] Whitney, J. and S. Smith, 1998, 'Observations on the Dynamic Performance of Tunnel Thrusters', In *OCEANS'98 IEEE Conference Proceedings*, Nice, France.

[18] Ridley, D., 1971, 'Observations on the Effect of Vessel Speed on Bow Thruster Performance', *Marine Technology*, 93–96.

[19] Blanke, M., K. Lingaard, and T. Fossen, 2000, 'Dynamic Model for Thrust Generation of Marine Propellers', In: *Conference on Marine Craft Maneuvering and Control*.